Int. J. Solids Structures Vol. 27, No. 13, pp. 1645–1662, 1991
Printed in Great Britain.

0020–7683/91 $3.00 + .00

PLANE STRAIN ANALYSIS OF A STATIONARY HYDRAULIC FRACTURE IN A POROELASTIC MEDIUM

EMMANUEL DETOURNAY
Schlumberger Cambridge Research, P.O. Box 153, Cambridge CB3 0HG, U.K.

and

ALEXANDER H.-D. CHENG
Department of Civil Engineering, University of Delaware, Newark, DE 19716, U.S.A.

(*Received* 31 *August* 1989; *in revised form* 5 *July* 1990)

Abstract—This paper presents a plane strain analysis of a constant length hydraulic fracture embedded in an infinite poroelastic domain. The fracture is uniformly loaded by fluid pressurization. For clarity of physical interpretation, this loading is decomposed into two modes, consisting respectively of a unit step for the normal stress and a unit step for the pore pressure along the fracture. For each loading mode, the transient fracture profile, the fracture volume, the leak-off volume, and the stress intensity factor are analyzed. First, short- and long-term asymptotic expressions are derived in closed form based on analytical arguments. The full transient behaviors are then formulated as a pair of coupled singular integral equations. The solutions are found via Laplace transform, and numerical discretization of the integral equations.

INTRODUCTION

This paper sets out to examine the fundamentals of the response of a stationary fracture embedded in an infinite, two-dimensional, poroelastic medium. The problem studied here is the sudden opening of a linear crack of length $2L$, at time $t = 0$, by a pressurized fluid which is kept at a constant pressure p_f for $t > 0$ (see Fig. 1). The time-dependent response of the fracture to this loading is analyzed on the basis of the following assumptions:

- the material behaves according to the linear poroelastic theory of Biot (1941), and is homogeneous and isotropic;
- deformation in the medium, induced by pressurization of the fracture, is subject to the condition of plane strain;
- before pressurization of the fracture, the initial state is characterized by a uniform compressive stress and pore pressure;
- the fracture is oriented in the direction perpendicular to the minimum compressive far-field stress;
- the fluid in the fracture and the pore fluid have identical rheological properties (i.e. viscosity and compressibility).

This analysis is motivated by the need to evaluate the impact of poroelastic effects during hydraulic fracturing treatments (a technique widely used by the oil and gas industry to enhance underground hydrocarbon recovery). This technique consists of injecting a fracturing fluid into a wellbore to initiate and propagate a fracture in the direction perpendicular to the *in situ* minimum compressive stress. Poroelastic effects, which reflect the interaction between deformation of the porous solid and diffusion of the pore fluid, are generally not taken into account in the current generation of hydraulic fracturing design codes (see e.g. a review in Mendelsohn, 1984a, b). There is, however, field evidence (Smith, 1985; Nierode, 1985) that the injection pressure is higher than that predicted by existing design models, when poroelastic effects appear to be important.

The objective of the present paper is to provide a basic understanding of the poroelastic processes in hydraulic fracturing via the idealized problem of a stationary fracture subject to a constant fluid pressure. This problem is the natural extension of the classical Griffith

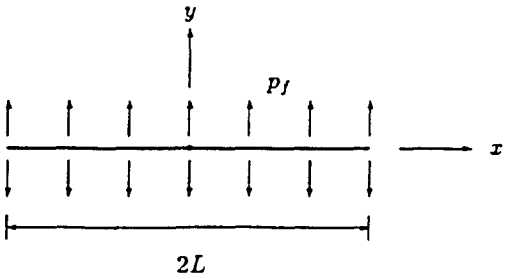

Fig. 1. A fluid-pressurized stationary fracture.

fracture problem in elasticity. In a companion paper (Cheng and Detournay, 1991), the idealized case of a steadily moving fracture will be examined.

The paper is organized as follows. It begins with a succinct presentation of the Biot theory of poroelasticity, followed by a description of the loading decomposition into two fundamental modes. The small and large time asymptotic behavior of the fracture response to the step loading is then examined using analytical arguments. Next, the transient problem is formulated as a pair of coupled singular integral equations. The numerical techniques of Laplace transform and inversion, and also discretization of the integral equations, are described. Numerical results for the evolution of the fracture profile, fracture volume, fluid leak-off volume, and stress intensity factor are then presented. This paper concludes with a discussion of the impact of poroelasticity on hydraulic fracturing treatment.

POROELASTICITY

The theory of poroelasticity introduced by Biot (1941) provides a simple consistent description of the coupled deformation/diffusion phenomena that characterize the response of fluid-saturated porous solids. As in the original formulation of Biot (see also Rice and Cleary, 1976), the constitutive equations are expressed here in terms of the total stress σ_{ij}, the pore pressure p, and their conjugate quantities which are respectively the solid strain e_{ij} (derivable from an average solid displacement vector u_i) and the variation of fluid content per unit reference volume ζ. For plane strain conditions, the constitutive equations of a linear isotropic poroelastic material can be written as

$$2Ge_{ij} = \sigma_{ij} - \nu\sigma_{kk}\delta_{ij} + \alpha(1-2\nu)\delta_{ij}p, \tag{1}$$

$$2G\zeta = \alpha(1-2\nu)\sigma_{kk} + \frac{\alpha^2(1-2\nu)^2}{\nu_u - \nu}p, \tag{2}$$

where the indices take the values 1 and 2, and repeated indices imply summation. The symbol δ_{ij} denotes the Kronecker delta.

The basic material constants introduced above are: the shear modulus G, the drained and undrained Poisson's ratios ν and ν_u, and the Biot coefficient α. Compared to an isotropic elastic material, two additional constants α and ν_u have thus been introduced. It can be shown (Geertsma, 1957; Rice and Cleary, 1976) that α is a characteristic of the solid skeleton only, while ν_u reflects the mechanical properties of both the fluid and solid constituent. Note that their range of variation is $0 < \alpha \leqslant 1$ and $\nu < \nu_u \leqslant 0.5$.

The parameters α and ν_u control the magnitude of two distinct poroelastic effects which are embodied in the constitutive equations (1) and (2):

- an increase of the pore pressure induces a dilation of the porous solid. This volumetric strain, e, is proportional to the Biot coefficient α and to the change of pore pressure as $2Ge = (1-2\nu)(\sigma_{kk} + 2\alpha p)$;
- under undrained conditions (corresponding to $\zeta = 0$), a perturbation of the pore pressure

is induced, which is proportional to the difference $\nu_u - \nu$ and the change of the mean stress, $p = -(\nu_u - \nu)\sigma_{kk}/\alpha(1-2\nu)$. From (1) we see that the material responds elastically, with the undrained Poisson's ratio ν_u, to variation of the mean stress, since $2Ge_{ij} = \sigma_{ij} - \nu_u \sigma_{kk}\delta_{ij}$.

The poroelastic effects described above are strongest when α and ν_u simultaneously assume their upper bound values. This limiting case occurs when the compressibility of both the fluid and solid constituents is much smaller than the compressibility of the porous solid skeleton (Rice and Cleary, 1976; Verruijt, 1969). Conversely, the contrast between drained and undrained response disappears in the case of a very compressible fluid (such as gas), since then $\nu_u \simeq \nu$.

Besides the constitutive equations (1) and (2), a complete description of the governing equations for poroelasticity consists also of:

the equilibrium equations

$$\sigma_{ij,j} = 0, \tag{3}$$

Darcy's law

$$q_i = -\kappa p_{,i}, \tag{4}$$

and the fluid mass balance equation

$$\frac{\partial \zeta}{\partial t} + q_{i,i} = 0, \tag{5}$$

where q_i is the specific discharge vector and κ the permeability coefficient, which can be expressed as k/μ, where k is the intrinsic permeability (dimension of length squared) and μ the fluid vicosity. In the above, we have neglected the existence of body forces and fluid sources.

The governing equations can be combined to yield field equations in terms of the displacement vector u_i and the pore pressure p. The resultant is a Navier equation with a coupling term:

$$G\nabla^2 u_i + \frac{G}{1-2\nu} u_{k,ki} - \alpha p_{,i} = 0, \tag{6}$$

and an inhomogeneous diffusion equation for p

$$\frac{\partial p}{\partial t} - \frac{c(1-2\nu)(1-\nu_u)}{(1-2\nu_u)(1-\nu)} \nabla^2 p + \frac{2G(\nu_u - \nu)}{\alpha(1-2\nu)(1-2\nu_u)} \frac{\partial u_{k,k}}{\partial t} = 0, \tag{7}$$

where c is a diffusivity coefficient given by

$$c = \frac{2\kappa G(1-\nu)(\nu_u - \nu)}{\alpha^2(1-2\nu)^2(1-\nu_u)}. \tag{8}$$

LOADING DECOMPOSITION

The application of a fluid pressure on the fracture wall actually corresponds to two non-zero boundary conditions, one for the normal stress, $\sigma_n = -p_f$, the other for the pore pressure, $p = p_f$. To account for the existence of a far-field stress (normal to the fracture) and a pore pressure with different magnitudes, the loading is decomposed into two fundamental modes:

- mode 1

$$\sigma_n(x,t) = -H(t),$$
$$p(x,t) = 0; \tag{9}$$

- mode 2

$$\sigma_n(x,t) = 0,$$
$$p(x,t) = H(t), \tag{10}$$

for $-L \leqslant x \leqslant L$. In the above, $H(t)$ denotes the Heaviside step function. The initial conditions for both problems are zero stress and pore pressure everywhere.

Once the solutions of the fundamental modes are found, the fracture responses such as maximum aperture opening, fracture volume and fluid leak-off volume can be expressed in the forms of response functions $\mathscr{F}_1$ and $\mathscr{F}_2$, respectively, for modes 1 and 2. In the presence of a far-field compressive stress σ_0 normal to the fracture and a pore pressure p_0, the actual response due to a constant fluid pressure p_f is calculated by a linear combination of the responses of mode 1 and mode 2:

$$\mathscr{F} = (p_f - \sigma_0)\mathscr{F}_1 + (p_f - p_0)\mathscr{F}_2. \tag{11}$$

Furthermore, for a transient pressurization $p_f = p_f(t)$, the fracture response can be obtained by a simple application of Duhamel's theorem

$$\mathscr{F}(t) = \mathscr{F}_1(t)[p_f(0^+) - \sigma_0] + \mathscr{F}_2(t)[p_f(0^+) - p_0] + \int_0^t [\mathscr{F}_1(t-\tau) + \mathscr{F}_2(t-\tau)] \frac{dp_f(\tau)}{d\tau}\, d\tau. \tag{12}$$

ASYMPTOTIC ANALYSIS

Before performing a full transient analysis of the pressurized crack, we discuss the asymptotic behavior of the two fundamental loading modes.

Mode 1 loading

Short-term response of the fracture volume. Just after application of the normal stress $\sigma_n = -1$ inside the crack (i.e. at $t = 0^+$), the medium responds elastically with undrained elastic moduli (see Rice and Cleary, 1976, for a discussion of the general short- and long-term behavior of a poroelastic system). The stress and displacement field are thus given by the solution of Sneddon (1946). In particular, the initial fracture opening is given by

$$D_n(x,0^+) = -\frac{2(1-\nu_u)}{G}\sqrt{L^2 - x^2}; \quad -L \leqslant x \leqslant L, \tag{13}$$

where D_n is the normal displacement discontinuity defined as

$$D_n(x,t) = u_y(x,0^-;t) - u_y(x,0^+;t); \quad -L \leqslant x \leqslant L. \tag{14}$$

The initial crack volume, $V_c^{(1)}(0^+)$, is calculated by integrating (13) over the crack length $(-L, L)$:

$$V_c^{(1)}(0^+) = \frac{\pi L^2(1-\nu_u)}{G}. \tag{15}$$

Consider next the early time evolution of the fracture volume. The undrained elastic response at $t = 0^+$ is associated with the instant generation of a pore pressure field

$$\lim_{t\to 0^+} p = -\frac{\nu_u - \nu}{\alpha(1-2\nu)} \lim_{t\to 0^+} (\sigma_{xx} + \sigma_{yy}). \tag{16}$$

At the fracture surface $\sigma_{xx} = \sigma_{yy} = -1$, hence

$$\lim_{t\to 0^+} p = \frac{2(\nu_u - \nu)}{\alpha(1-2\nu)}; \quad y = 0, \quad -L \leqslant x \leqslant L. \tag{17}$$

This initial value of p along the boundary is not in equilibrium with the imposed boundary condition $p = 0$ and must be dissipated. At small times the diffusion process at the crack surface is approximately one-dimensional. As demonstrated in the subsequent mode 2 analysis, there is a fracture volume change associated with this one-dimensional diffusion process. This incremental volume change is calculated by multiplying the magnitude of pressure $-2(\nu_u - \nu)/\alpha(1-2\nu)$, see (17), by the right-hand side of (32) (which gives the early time fracture volume reduction associated with a unit pore pressure on the fracture surface). Combining this incremental volume change with the initial contribution (15), the small time fracture volume is therefore given by

$$V_c^{(1)}(t) = \frac{\pi L^2(1-\nu_u)}{G} + \frac{16L^2(1-\nu_u)(\nu_u - \nu)}{G\sqrt{\pi}(1-\nu)}\sqrt{\frac{ct}{L^2}}; \quad \text{for} \quad \sqrt{\frac{ct}{L^2}} \ll 1. \tag{18}$$

Long-term limit of the fracture volume. As time approaches infinity, the pore pressure induced by loading of the crack has completely vanished and the medium responds elastically. The crack opening is again described by the Sneddon's solution (15), but with the drained Poisson's ratio substituted for the undrained one:

$$V_c^{(1)}(\infty) = \frac{\pi L^2(1-\nu)}{G}. \tag{19}$$

The final aperture is thus greater than the initial one; this is to be expected since the poroelastic material is softer when drained. Between $t = 0^+$ and $t = \infty$, the fracture will thus experience a progressive time-dependent volume increase of the amount

$$\Delta V_c^{(1)} = \frac{\pi L^2(\nu_u - \nu)}{G}. \tag{20}$$

Short-term response of the leak-off volume. As discussed above, at $t = 0^+$ a pore pressure field (16) is instantly generated, which must be dissipated. At very small times ($ct/L^2 \ll 1$), the fluid flux near the fracture surface is predominantly one-dimensional. Since the diffusion equation for pressure (7) becomes uncoupled in a one-dimensional geometry, the fluid flux for a unit pressure drop is given by

$$q_y = \frac{\kappa}{\sqrt{\pi ct}}; \quad y = 0, \quad -L \leqslant x \leqslant L. \tag{21}$$

Integrating this solution over time, multiplying by $4L$ (the total crack face length) and by the initial pore pressure drop (17), yields the cumulative fluid leak-off volume:

$$V_l^{(1)}(t) = -\frac{8\alpha L^2(1-2\nu)(1-\nu_u)}{G\sqrt{\pi}(1-\nu)}\sqrt{\frac{ct}{L^2}}; \quad \text{for} \quad \frac{ct}{L^2} \ll 1. \tag{22}$$

The negative sign indicates that fluid is extracted from the medium.

Long-term limit of the leak-off volume. Integrating the fluid mass balance equation (5) over time and over the domain, and applying the divergence theorem to the flux term, we observe that the leak-off volume can be evaluated as the integration of the variation of fluid content per unit volume ζ over the domain. In particular, in the long-term limit ($t \to \infty$)

$$V_l^{(1)}(\infty) = 2\int_0^{\infty}\int_{-L}^{+L} q_y \, dx \, dt = \int_V \zeta|_{t=\infty} \, dV \tag{23}$$

where $\int_V dV$ denotes domain integration. In the above we have utilized the condition that no fluid is exchanged with infinity due to the favorable pore pressure field induced at $t = 0^+$ ($p \sim 1/r^2$ as $r \to \infty$, thus $q_r \sim 1/r^3$, where r is the radial distance from the origin).

From the poroelastic constitutive equations (1) and (2), it can be shown that when all excess pore pressure is dissipated (at time equal to infinity), ζ is related to the solid dilatation e as

$$\lim_{t\to\infty}\zeta = \alpha \lim_{t\to\infty} e. \tag{24}$$

Instead of directly performing the domain integration, the integral of e can be evaluated as a volume change of the fracture. The final fracture volume $V_c^{(1)}(\infty)$ given in (19) consists of contributions from volumetric and deviatoric strains in the medium. The latter contribution is simply computed by setting ν to 1/2 into (19), giving $\pi L^2/2G$. The volumetric strain contribution to $V_c^{(1)}(\infty)$ is then calculated as the difference. All calculations done, the final fluid volume exchanged between the medium and the fracture is:

$$V_l^{(1)}(\infty) = -\frac{\alpha\pi L^2(1-2\nu)}{2G}. \tag{25}$$

Short- and long-term limit of the stress intensity factor. Consider first the long-term value of the stress intensity factor. As time $t \to \infty$, the medium responds as a drained elastic material. From the classical solution, the stress intensity factor (SIF) is given by

$$K_I^{(1)}(\infty) = \sqrt{\pi L}. \tag{26}$$

It is of interest to note that the above quantity is independent of any material property.

The initial value of the SIF is reduced with respect to its long-term value by a factor $(1-\nu_u)/(1-\nu)$. This reduction of the SIF is explained using the following heuristic argument, which is based on the results of Rice and Simons (1976) and Simons (1977) for steadily moving semi-infinite cracks. At time $t = 0^+$, the medium responds elastically (with an undrained Poisson's ratio) and a pore pressure field is induced around the crack. This initial pore pressure is, however, characterized by infinite gradients at the tips, with the consequence that the pore pressure at the tips vanishes at $t > 0$ (in other words, the crack tips are effectively drained at $t > 0$). Since the $r^{-1/2}$ stress singularity is preserved (Rice and Simons, 1976; Simons, 1977), the classical elastic relationship between the crack opening displacement and the SIF applies therefore at all times:

$$K_I = \frac{\sqrt{\pi}G}{\sqrt{8}(1-\nu)}\lim_{\xi\to 0}\frac{D_n}{\sqrt{\xi}}, \tag{27}$$

where

$$\xi = L - |x|. \tag{28}$$

Substituting D_n in (27) by its initial value [given by (13)], it can be seen that the small time value of the SIF is

$$K_I^{(1)}(0^+) = \frac{1-\nu_u}{1-\nu}\sqrt{\pi L}. \tag{29}$$

Mode 2 loading

Short- and long-term response of the fracture volume. Using the theorem of reciprocity of work, it is first proven that the mode 2 fracture volume is actually equal to the mode 1 fluid leak-off volume. From the reciprocal theorem of poroelasticity (Cheng and Predeleanu, 1987; Cleary, 1977) [see also Nowacki (1986) for the equivalent thermoelastic theorem], the following boundary integral equation can be written in a domain free from initial disturbances

$$\int_S [t_i^{(1)}(\chi; t)u_i^{(2)}(\chi; t) - t_i^{(2)}(\chi; t)u_i^{(1)}(\chi; t)]\,\mathrm{d}S(\chi)$$

$$-\int_S [p^{(1)}(\chi; t)v^{(2)}(\chi; t) - p^{(2)}(\chi; t)v^{(1)}(\chi; t)]\,\mathrm{d}S(\chi) = 0. \tag{30}$$

In the above, $t_i = \sigma_{ij}n_j$ is the boundary traction vector, with n_j denoting the components of the unit outward normal to the boundary; $v = \int_0^t q_i n_i\,\mathrm{d}t$ is the fluid displacement vector normal to the boundary; S is the boundary of the solution domain; and the superscripts (1) and (2) mark quantities of two independent poroelastic states. Here, these two states are associated with loading modes 1 and 2, and the boundary refers to the fracture faces.

Substituting the boundary conditions (9) and (10) in (30) and performing the integration, it is apparent that the mode 2 fracture volume is equal to the mode 1 fluid leak-off volume at all times:

$$V_c^{(2)} = V_l^{(1)}. \tag{31}$$

From the mode 1 results, we directly obtain that

$$V_c^{(2)}(t) = -\frac{8\alpha L^2(1-2\nu)(1-\nu_u)}{G\sqrt{\pi}(1-\nu)}\sqrt{\frac{ct}{L^2}}; \quad \text{for} \quad \frac{ct}{L^2} \ll 1, \tag{32}$$

$$V_c^{(2)}(\infty) = -\frac{\alpha\pi L^2(1-2\nu)}{2G}. \tag{33}$$

The above values are negative, indicating that mode 2 loading induces a "closure" of the fracture (of course, it is assumed that the crack remains open under combined mode 1 and 2 loading). This closure is the result of the dilatation of the porous solid around the fracture, caused by the increase of pore pressure.

It is also of interest to examine the long-term limit of fracture volume, $V_c^{(2)}(\infty)$, from a different perspective. At large times, the pore pressure in the region surrounding the fracture reaches a near constant value (characterized by axial symmetry). In the absence of a fracture cut, this pore pressure would have induced an irrotational displacement field. It can be shown (see Appendix A) that under these circumstances the stress field is directly related to the pore pressure by

$$\frac{\sigma_{xx}+\sigma_{yy}}{2} = -\eta p. \tag{34}$$

As $t \to \infty$, the pore pressure p in the region around the fracture approaches the asymptotic value of 1, and a uniform confining stress develops:

$$\sigma_{xx} = \sigma_{yy} = -\eta; \quad \text{as} \quad t \to \infty. \tag{35}$$

To impose the condition of a fracture with zero stresses on the surface, the solution of an internally-loaded Griffith fracture in a drained medium ($\sigma_{yy} = \eta$ and $\sigma_{xy} = 0$, at $-L \leqslant x \leqslant L$, $y = 0$; and $p = 0$ everywhere) is superposed. The final fracture volume is equal to that created by the second problem, and is calculated as the Sneddon solution (19) multiplied by the factor $-\eta$. The result is identical to (33). The long-term effect on the fracture volume caused by a unit rise of the pore pressure is therefore equivalent to the application of a tensile stress $\sigma^B = \eta$ on the fracture faces. This stress has been called the "back-stress" by Cleary (1980).

Short- and long-term response of the leak-off volume. Early after application of the step pressure, a one-dimensional flow perpendicular to the fracture faces takes place. The early time behavior of the fluid leak-off volume can thus again be derived from expression (21), and is given by

$$V_l^{(2)}(t) = \frac{8\kappa L^2}{c\sqrt{\pi}}\sqrt{\frac{ct}{L^2}}; \quad \text{for} \quad \frac{ct}{L^2} \ll 1. \tag{36}$$

At large times, the diffusion takes a "pseudo-radial" pattern. Following the earlier argument, eqn (7) uncouples to become a homogeneous diffusion equation (A1) [$f(t) = 0$ because of the medium being infinite]. The large time leak-off volume can be obtained from the classical solution of a steep rise of pressure on the perimeter of a circular hole (Carslaw and Jaeger, 1959):

$$V_l^{(2)}(t) = \frac{8\kappa}{\pi}\int_0^t \frac{e^{-cu^2 t}}{cu^3[J_0^2(au)+Y_0^2(au)]}\,du; \quad \text{for} \quad \frac{ct}{L^2} \gg 1. \tag{37}$$

In the above, J_0 and Y_0 are Bessel functions of the first and second kind, respectively, and $a = 2L/\pi$ is the "equivalent radius".

Short- and long-term limit of the stress intensity factor. At time $t = 0^+$, there is no displacement on the crack face induced by mode 2 loading. Consequently,

$$K_I^{(2)}(0^+) = 0. \tag{38}$$

At time $t = \infty$, the deformation of the fracture surface is equivalent to the application of a normal stress equal to η. It follows therefore that

$$K_I^{(2)}(\infty) = -\eta\sqrt{\pi L}. \tag{39}$$

Here again the negative SIF should be interpreted as a reduction of the (positive) stress intensity factor due to mode 1 loading.

INTEGRAL EQUATION FORMULATION

The transient solution is obtained using an integral equation technique. The concept is described below. A hydraulic fracture in a poroelastic medium is a surface across which

the solid displacements and the normal fluid flux are discontinuous. Such a discontinuity surface can mathematically be simulated by a distribution over time and space of impulse point displacement discontinuities (DD) and sources. If the density of these singularities is known, integral representations of the field quantities, such as displacement, flux, stress and pore pressure, can be evaluated using the principle of superposition. In particular, for a linear fracture pressurized by a fluid, the integral representations of the normal stress and pore pressure on the crack surface are (Detournay and Cheng, 1987; Vandamme *et al.*, 1989):

$$\sigma_n(x,t) = \int_0^t \int_{-L}^{+L} D_n(\chi,\tau)\sigma_{nn}^{di}(x-\chi,t-\tau) + D_f(\chi,\tau)\sigma_{nf}^{si}(x-\chi,t-\tau)\,d\chi\,d\tau,$$

$$p(x,t) = \int_0^t \int_{-L}^{+L} D_n(\chi,\tau)p_n^{di}(x-\chi,t-\tau) + D_f(\chi,\tau)p_f^{si}(x-\chi,t-\tau)\,d\chi\,d\tau, \tag{40}$$

where $\sigma_n = \sigma_{yy}$ denotes the normal stress on the fracture, D_n is the normal displacement discontinuity density defined earlier, and D_f is the flux discontinuity density (source density, or the rate of fluid leak-off per unit fracture length). The quantities marked with superscripts "di" and "si" are the influence functions of an instantaneous point displacement discontinuity, and an instantaneous source, respectively: σ_{nn}^{di} is the normal stress and p_n^{di} the pressure generated by a unit normal displacement discontinuity; σ_{nf}^{si} and p_f^{si} are those caused by a unit fluid source. It should be remarked that the kernel functions in (40) contain hypersingularities, $1/(x-\chi)^2$. The integration is meaningful only if it is interpreted in the sense of the Hadamard principal value (Hadamard, 1952; Hong and Chen, 1988).

To facilitate the numerical solution, the Laplace transformation is applied to (40); and to reduce the level of singularity in the kernels, an integration by parts is performed on the terms containing the displacement discontinuity

$$\tilde{\sigma}_n(x,s) = \int_{-L}^{+L} \tilde{D}_n'(\chi,s)\tilde{\sigma}_{nn}^{ci}(x-\chi,s) + \tilde{D}_f(\chi,s)\tilde{\sigma}_{nf}^{si}(x-\chi,s)\,d\chi,$$

$$\tilde{p}(x,s) = \int_{-L}^{+L} \tilde{D}_n'(\chi,s)\tilde{p}_n^{ci}(x-\chi,s) + \tilde{D}_f(\chi,s)\tilde{p}_f^{si}(x-\chi,s)\,d\chi, \tag{41}$$

where the tilde overbar denotes the Laplace transform. In the above equations, $\tilde{D}_n' = \partial\tilde{D}_n/\partial\chi$ is the slope of the fracture profile, and

$$\tilde{\sigma}_{nn}^{ci}(x-\chi,s) = \int_{-\infty}^{\chi} \tilde{\sigma}_{nn}^{di}(x-\chi',s)\,d\chi', \tag{42}$$

is the influence function of normal stress due to an instantaneous normal "edge dislocation" (a fracture with a constant normal displacement discontinuity extending from $-\infty$ to χ). The kernel $\tilde{p}_n^{ci}$ is defined similarly. Also, to take care of the free term which results from this integration, an auxiliary condition of fracture closure is introduced

$$0 = \int_{-L}^{+L} \tilde{D}_n'(\chi,s)\,d\chi. \tag{43}$$

The poroelastic edge dislocation and fluid source influence functions can be obtained using a variable decomposition scheme originally suggested by Biot (1956) [see Detournay and Cheng (1987) for details]:

$$\tilde{\sigma}_{nn}^{ci} = \frac{G}{2\pi(1-\nu)}\frac{1}{x-\chi} - \frac{G(\nu_u-\nu)}{\pi(1-\nu_u)(1-\nu)}\left[\frac{K_{2-2}(z)}{x-\chi} + \sqrt{\frac{s}{c}}\frac{|x-\chi|}{x-\chi}K_{1-1}(z)\right],$$

$$\tilde{\sigma}_{nf}^{si} = \frac{\eta}{2\pi\kappa}\left[\ln|x-\chi| - K_{2-1}(z) - K_{0-1}(z) + \ln\sqrt{\frac{s}{c}}\right],$$

$$\tilde{p}_n^{ci} = \frac{G(\nu_u-\nu)}{2\pi\eta(1-\nu_u)(1-\nu)}\sqrt{\frac{s}{c}}\frac{|x-\chi|}{x-\chi}K_{1-1}(z),$$

$$\tilde{p}_f^{si} = \frac{1}{2\pi\kappa}\left[-\ln|x-\chi| + K_{0-1}(z) - \ln\sqrt{\frac{s}{c}}\right]. \tag{44}$$

In the foregoing, $z = \sqrt{s/c}\,|x-\chi|$, and K_{0-1}, K_{1-1}, etc., are the modified Bessel functions of second kind without the leading terms:

$$K_{0-1}(z) = K_0(z) + \ln z,$$

$$K_{1-1}(z) = K_1(z) - \frac{1}{z},$$

$$K_{2-1}(z) = K_2(z) - \frac{2}{z^2},$$

$$K_{2-2}(z) = K_2(z) - \frac{2}{z^2} + \frac{1}{2}. \tag{45}$$

The above quantities are non-singular.

In order to accurately represent the limiting behavior of $\tilde{D}_n'$ near the crack tips ($\tilde{D}_n' \sim \xi^{-1/2}$, where ξ is the distance from the tip), $\tilde{D}_n'$ is factored by a shape function

$$\tilde{D}_n'(\chi, s) = \frac{\phi(\chi, s)}{\sqrt{L^2-\chi^2}}. \tag{46}$$

The solution of $\phi(\chi, s)$ is therefore regular at crack tips and can be computed with high accuracy. The stress intensity factor is then evaluated as

$$\tilde{K}_I(s) = \pm\frac{G\sqrt{\pi}}{2(1-\nu)}\phi(\pm L, s). \tag{47}$$

Substituting (44) and (46) into (41) and rearranging, we obtain

$$\begin{aligned}\tilde{\sigma}_n(x, s) = {} & \frac{G}{2\pi(1-\nu)}\int_{-L}^{+L}\frac{\phi(\chi, s)}{(x-\chi)\sqrt{L^2-\chi^2}}\,d\chi \\ & + \frac{\eta}{2\pi\kappa}\int_{-L}^{+L}\tilde{D}_f(\chi, s)\ln|x-\chi|\,d\chi \\ & - \frac{G(\nu_u-\nu)}{\pi(1-\nu_u)(1-\nu)}\int_{-L}^{+L}\frac{\phi(\chi, s)F_1(x-\chi, s)}{\sqrt{L^2-\chi^2}}\,d\chi \\ & - \frac{\eta}{2\pi\kappa}\int_{-L}^{+L}\tilde{D}_f(\chi, s)F_2(x-\chi, s)\,d\chi;\end{aligned}$$

$$\tilde{p}(x,s) = -\frac{1}{2\pi\kappa}\int_{-L}^{+L}\tilde{D}_1(\chi,s)\ln|x-\chi|\,d\chi + \frac{G(\nu_u-\nu)}{2\pi\eta(1-\nu_u)(1-\nu)}\int_{-L}^{+L}\frac{\phi(\chi,s)F_3(x-\chi,s)}{\sqrt{L^2-\chi^2}}\,d\chi + \frac{1}{2\pi\kappa}\int_{-L}^{+L}\tilde{D}_1(\chi,s)F_4(x-\chi,s)\,d\chi; \tag{48}$$

where F_1–F_4 are the non-singular parts of the influence functions

$$F_1 = \frac{K_{2,-2}(z)}{x-\chi} + \sqrt{\frac{s}{c}}\frac{|x-\chi|}{x-\chi}K_{1,-1}(z),$$

$$F_2 = K_{2,-1}(z) + K_{0,-1}(z) - \ln\sqrt{\frac{s}{c}},$$

$$F_3 = \sqrt{\frac{s}{c}}\frac{|x-\chi|}{x-\chi}K_{1,-1}(z),$$

$$F_4 = K_{0,-1}(z) - \ln\sqrt{\frac{s}{c}}. \tag{49}$$

The two integral equations in (48) are respectively Cauchy ($1/r$) and logarithmic singular, for nodes located on the crack, but not at the tips.

Equations (48) and (43) can be exploited by a numerical algorithm to solve for $\tilde{\phi}$ and $\tilde{D}_1$. The details are described in Appendix B.

RESULTS

We present below some transient numerical results for modes 1 and 2, which are compared with the available asymptotic solutions. The material constants used for these examples are $\nu = 0.2$, $\nu_u = 0.4$ and $\alpha = 0.89$ (or the Skempton pore pressure coefficient $B = 0.8$). The solutions, when properly non-dimensionalized, are otherwise independent of the rest of the parameters. The crack length $2L$ is discretized using six quadratic elements of equal size. The numerical Laplace inversion was performed with six terms in the Stehfest series.

Figure 2 displays the mode 1 fracture opening profile as a function of the dimensionless time $t^* = ct/L^2$. Due to symmetry, only half of the geometry is plotted. The small and large

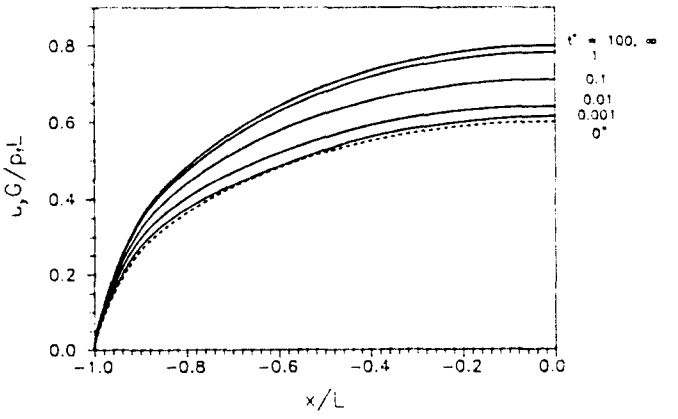

Fig. 2. Mode 1 fracture profile.

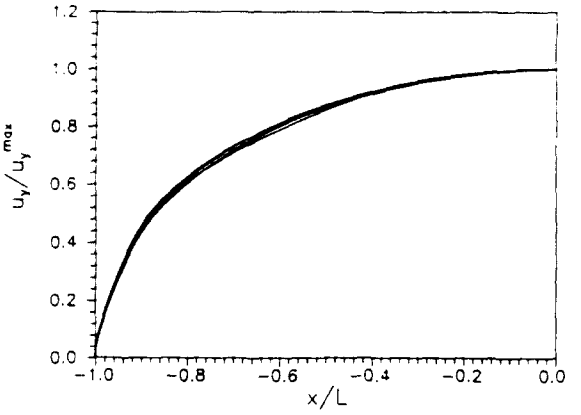

Fig. 3. Mode I normalized fracture profile.

time asymptotic profiles, which are ellipses according to the elastic solution, (13), are shown by dashed lines (the large time asymptotic solution is indistinguishable from the $t^* = 100$ result). We observe that the poroelastic solution does approach these limits and that the transient fracture profiles are remarkably elliptic.

Figure 3 shows the same fracture profiles as in Fig. 2, but each normalized by their maximum opening. The resultant curves seem to collapse into a single curve with only a slight fuzziness.

Figure 4 plots the negative of the fracture profile for mode 2. As can be seen, the fracture has not reached its theoretical maximum closure even at $t^* = 100$. This slow convergence is a characteristic for diffusion in an infinite domain. In fact, the near steady state solution is not attainable in realistic terms.

Figure 5 presents the mode 2 normalized fracture profile. The profile at small times is not elliptic, although it approaches that shape fairly rapidly and becomes practically an ellipse for $t^* > 1$.

Figure 6 displays the mode I fracture volume response, which is observed to increase with time. Also plotted are small and large time asymptotic behaviors, (18) and (19) in dashed lines. The small time asymptotic result appears to be an excellent approximation for $t^* < 0.001$.

Figure 7 shows both the negative mode 2 fracture volume and the negative mode I fluid leak-off volume. As indicated earlier, these quantities should be identical. This claim is indeed supported by the numerical results as only a single curve appeared in Fig. 7. The

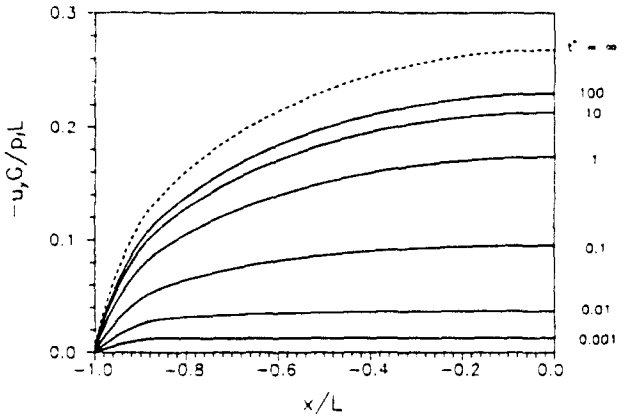

Fig. 4. Mode 2 fracture profile.

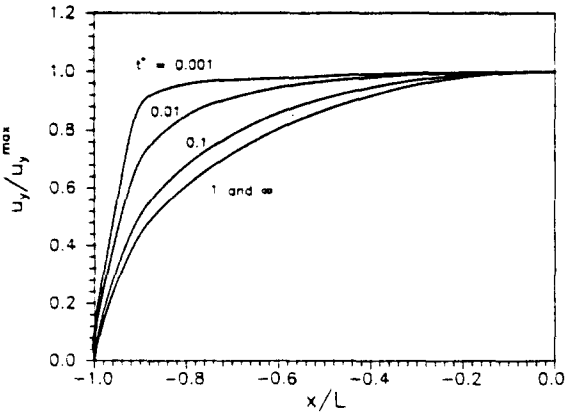

Fig. 5. Mode 2 normalized fracture profile.

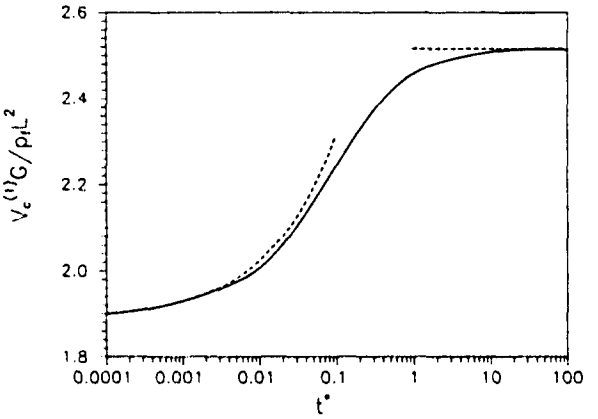

Fig. 6. Mode 1 fracture volume.

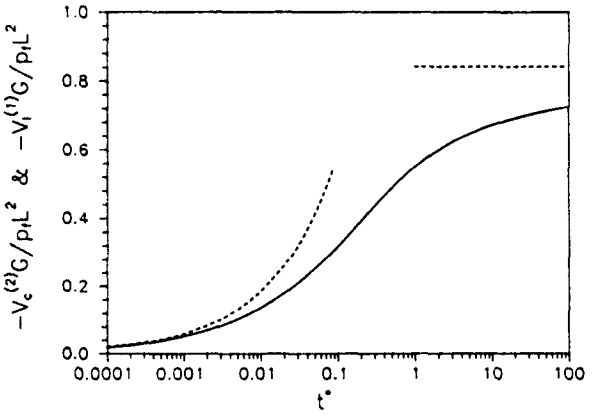

Fig. 7. Mode 1 fluid leak-off volume and mode 2 fracture volume.

small and large time asymptotic behaviors, (32) and (33), are shown by dashed lines. The large time asymptotic solution is far from being reached as compared with the mode 1 fracture volume case (Fig. 6). This discrepancy may be attributed to the time required for the diffusion to reach steady state in the two cases. In the mode 1 case, the pore pressure is generated in the near-crack region and diminishes toward infinity; it is more easily dissipated. For mode 2, the medium is initially free from pore pressure. As the pressure front propagates into the medium, the flux on the fracture faces decreases as $t^{-1/2}$ due to diminishing pressure gradient in the near field. The mode 2 curve therefore lags far behind its limiting value in the range of the plot.

Figure 8 presents the mode 2 fluid leak-off volume. The solution is unbounded. The one-dimensional small time approximation (36), plotted as a lower bound by the dashed line, follows the curve fairly well for a range of time. The large time solution (37), shown as an upper bound by the dashed line, is based on a circular hole geometry and uncoupled diffusion equation. It is somewhat surprising to observe that this solution is a good approximation throughout time.

Figures 9 and 10 give the stress intensity factors for modes 1 and 2, respectively (negative SIF in the mode 2 case). The limiting values given as (26), (29) and (39) are shown by dashed lines.

SUMMARY AND CONCLUSION

In this paper, the basic response of a stationary hydraulic fracture in an infinite poroelastic medium has been presented. The solution may be viewed as an extension of the classical problem of a Griffith crack in an elastic medium. The analysis begins with asymptotic solutions which are based on the limiting elastic and diffusion behaviors. The full transient solution requires an integral equation technique which makes use of a continuous distribution of poroelastic dislocation and source singularities along the fracture. The solution is found by Laplace transform and inversion, and numerical discretization.

The fluid pressurization in the fracture is viewed here as a superposition of two modes, the first one corresponding to the application of a normal stress on the fracture wall, the second to a pore pressure. This decomposition is carried out not only for the convenience of the mathematical solution in the presence of an initial stress σ_0 and initial pore pressure p_0, but also because it brings physical insight into two distinct processes.

Motivated by considerations regarding hydraulic fracturing treatments, we have emphasized the calculation of "global" quantities that are important to the fracture design: the fracture volume V_f, the fluid leak-off volume V_l, and the stress intensity factor K_I. The first two quantities are associated with the amount of fracturing fluid required in the treatment, and the last provides information concerning the fracture propagation criterion. The local quantities, such as stress, displacement, flux, etc., though not explicitly presented here, can also be calculated from the integral equations.

The present analysis, although simplistic in its assumptions, provides some important guidelines concerning poroelastic effects in hydraulic fracturing. Some of these are discussed below.

- Mode 1 loading indicates that the fracture volume (and also the aperture width) increases as a function of treatment time. The mode 2 effects, however, predict a closure. The final variation of fracture volume, combining both modes 1 and 2, is

$$\Delta V_c = \frac{\pi L^2}{G}\left[(p_f-\sigma_0)(v_u-v)-(p_f-p_0)\frac{\alpha(1-2v)}{2}\right]. \tag{50}$$

For realistic stresses and material parameters in oil-bearing formations, the above value is typically negative, indicating a reduction in aperture width with time. In the present analysis, the fracturing pressure is assumed to be constant on the fracture faces. In the actual operation, the pressure is controlled by the pumping rate, the leak-off into the formation, and the aperture width which introduces a resistance to the viscous fluid.

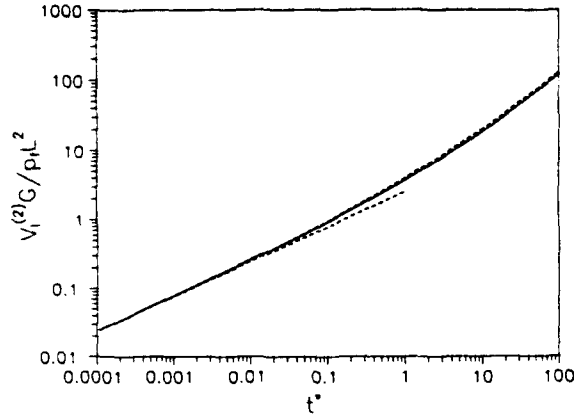

Fig. 8. Mode 2 fluid leak-off volume.

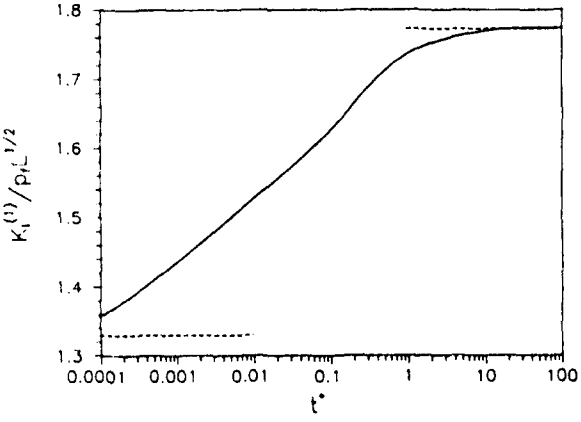

Fig. 9. Mode 1 stress intensity factor.

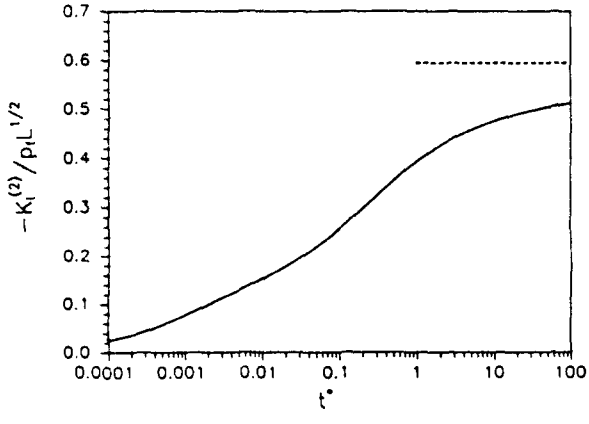

Fig. 10. Mode 2 stress intensity factor.

When poroelasticity is incorporated into a hydraulic fracturing design model, a higher fracturing pressure is predicted (Detournay *et al.*, 1990).

- The fluid efflux into the formation (leak-off) is dominated by the mode 2 component, as mode 1 only creates a small amount of influx which slightly impedes the mode 2 process. We also discovered that the poroelastic coupling effect is weak in mode 2. The leak-off volume calculated via poroelastic theory is nearly identical to that computed by the uncoupled diffusion equation. It should be pointed out, however, that in the present analysis the fracturing fluid is assumed to be of identical property to that of the reservoir fluid. In reality, the contrast of rheology properties between the two fluids and also the formation of the filter cake on the fracture surface calls for a more sophisticated treatment of the pressure boundary condition.
- A technique known as micro-hydraulic fracturing is widely used in the industry for *in situ* stress determination (Abou-Sayed *et al.*, 1978). In this test, fluid is injected into a borehole to create a small fracture and then the valve is shut off to lock the fluid in the cavity. As the fluid gradually permeates into the formation, the fracture closes and a fracture closure pressure p_{foc} may be interpreted from the pressure log. Equating this quantity to the minimum *in situ* stress σ_0 is only correct for impermeable rocks. For permeable formation, the result of the present analysis can be used to demonstrate that the actual relation involves the magnitude of the net stress $p_f - \sigma_0$, the net pressure $p_f - p_0$, poroelastic parameters ν_u and α, and the pressurization time (Detournay *et al.*, 1989).

Acknowledgements—The authors would like to thank Dowell Schlumberger for permission to publish these results, and Mr T. Badmus for his help in the numerical implementation of the integral equation technique.

REFERENCES

Abou-Sayed, A. S., Brechtel, C. E. and Clifton, R. J. (1978). *In situ* stress determination by hydrofracturing: a fracture mechanics approach. *J. Geophys. Res.* **83**, 2851–2862.

Biot, M. A. (1941). General theory of three-dimensional consolidation. *J. Appl. Phys.* **12**, 155–164.

Biot, M. A. (1956). General solutions of the equations of elasticity and consolidation for a porous material. *J. Appl. Mech., Trans. ASME* **78**, 91–96.

Carslaw, H. S. and Jaeger, J. C. (1959). *Conduction of Heat in Solids*, 2nd ed. Oxford University Press (Clarendon), London.

Cheng, A. H.-D. and Predeleanu, M. (1987). Transient boundary element formulation for poroelasticity. *Appl. Math. Modelling* **11**, 285–290.

Cheng, A. H.-D. and Detournay, E. (1991). Plane strain analysis of a steadily moving fracture in a poroelastic medium. Manuscript in preparation.

Cleary, M. P. (1977). Fundamental solutions for a fluid-saturated porous solid. *Int. J. Solids Structures* **13**, 785–806.

Cleary, M. P. (1980). Analysis of mechanisms and procedures for producing favorable shapes of hydraulic fractures. SPE paper 9260, *Proc. 55th Annual Fall Meeting*, SPE-AIME, Dallas.

Detournay, E. and Cheng, A. H.-D. (1987). Poroelastic solution of a plane strain point displacement discontinuity. *J. Appl. Mech.* **54**, 783–787.

Detournay, E., Cheng, A. H.-D. and McLennan, J. D. (1990). A poroelastic PKN hydraulic fracture model based on an explicit moving mesh algorithm. *J. Energy Res. Tech., ASME*, in print.

Detournay, E., Cheng, A. H.-D., Roegiers, J.-C. and McLennan, J. D. (1989). Poroelastic considerations in *in situ* stress determination by hydraulic fracturing. *Int. J. Rock Mech. Mining Sci. Geomech. Abstr.* **26**, 507–513.

Erdogan, F., Gupta, G. D. and Cook, T. S. (1973). Numerical solution of singular integral equations. In *Mechanics of Fracture 1: Methods of Analysis and Solutions of Crack Problems* (Edited by G. C. Sih), pp. 368–425. Noordhoff.

Geertsma, J. (1957). The effect of fluid pressure decline on volumetric changes of porous rocks. *Petroleum Trans., AIME* **210**, 331–340.

Gerasoulis, A. (1982). The use of piecewise quadratic polynomials for the solution of singular integral equations of the Cauchy type. *Comp. Math. Applics.* **8**, 15–22.

Hadamard, J. (1952). *Lectures on Cauchy's Problem in Linear Partial Differential Equations*. Dover, New York.

Hong, H. K. and Chen, J. T. (1988). Derivations of integral equations of elasticity. *J. Engng Mech., ASCE* **114**, 1028–1044.

de Josselin de Jong, G. (1963). Consolidatie in drie dimensies. *LGM-Mededelingen* **7**, 25–73.

Mendelsohn, D. A. (1984a). A review of hydraulic fracture modeling—Part I: General concepts, 2D models, motivation for 3D modeling. *J. Energy Res. Tech.* **106**, 369–376.

Mendelsohn, D. A. (1984b). A review of hydraulic fracture modeling—Part II: 3D modeling and vertical growth in layered rock. *J. Energy Res. Tech.* **106**, 543–553.

Nierode, D. E. (1985). Comparison of hydraulic fracture design methods to observed field results. *J. Pet. Tech.* 1831–1839.

Nowacki, W. (1986). *Thermoelasticity*, 2nd ed. Pergamon Press, London.

Parihar, K. S. and Ramachandran, M. P. (1986). Piecewise cubic interpolatory polynomials and approximate solution of singular integral equations. *Comp. Math. Applics.* **12A**, 1201–1215.
Rice, J. R. and Cleary, M. P. (1976). Some basic stress-diffusion solutions for fluid saturated elastic porous media with compressible constituents. *Rev. Geophys. Space Phys.* **14**, 227–241.
Rice, J. R. and Simons, D. A. (1976). The stabilization of spreading shear faults by coupled deformation–diffusion effect in fluid-infiltrated porous materials. *J. Geophys. Res.* **81**, 5322–5334.
Simons, D. A. (1977). Boundary layer analysis of propagating mode II cracks in porous elastic solids. *J. Mech. Phys. Solids* **25**, 99–116.
Smith, M. B. (1985). Stimulation design for short, precise hydraulic fractures. *Soc. Pet. Eng. Jl* 371–379.
Sneddon, I. N. (1946). The distribution of stress in the neighborhood of a crack in a elastic solid. *Proc. R. Soc.* **A187**, 229–260.
Stehfest, H. (1970). Numerical inversion of Laplace transforms. *CACM* **13**, 47–49 and 624.
Theocaris, P. S. and Ioakimidis, N. (1977). Numerical integration methods for the solution of singular integral equations. *Q. Appl. Math.* **35**, 173–182.
Vandamme, L., Detournay, E. and Cheng, A. H.-D. (1989). A two-dimensional poroelastic displacement discontinuity method for hydraulic fracture simulation. *Int. J. Numer. Anal. Meth. Geomech.* **13**, 215–224.
Verruijt, A. (1969). Elastic storage of aquifers. In *Flow Through Porous Media* (Edited by R. J. M. DeWiest). Academic Press, New York.
IMSL Inc. (1985). *IMSL Library User's Manual.*

APPENDIX A: IRROTATIONAL CONDITION

It has previously been noted by Biot (1956) and de Josselin de Jong (1963) that under a irrotational displacement condition, equation (7) uncouples from the displacement to become

$$\frac{\partial p}{\partial t} - c\nabla^2 p = f(t), \tag{A1}$$

where $f(t)$ is a function of time. With the exception of the one-dimensional problem and problems with unbounded domain, $f(t)$ is generally unknown. When $f(t)$ is zero, the system of (6) and (A1) is equivalent to the theory of thermal stress (uncoupled thermoelasticity).

After some manipulation, we find for plane strain that the following stress pressure relation exists

$$\sigma_{kk} = -2\eta p + g(t), \tag{A2}$$

where

$$\eta = \frac{\alpha(1-2\nu)}{2(1-\nu)} \tag{A3}$$

is a poroelasticity coefficient with the range $0 \leqslant \eta \leqslant 0.5$, and $g(t)$ is again an unknown function of time. For the current problem, which involves an unbounded domain, we can locate a point at infinity where both σ_{kk} and p vanish. The function $g(t)$ hence has to be zero everywhere.

APPENDIX B: NUMERICAL IMPLEMENTATION

To find an approximate solution of the integral equations (48) and (43), $\tilde{\phi}$ and $\tilde{D}_t$ can either be expressed as continuous functions such as Chebyshev or Lobatto–Chebyshev polynomials (Erdogan *et al.*, 1973; Theocaris and Ioakimidis, 1977), or be represented as piecewise continuous functions (Gerasoulis, 1982; Parihar and Ramachandran, 1986). In the present implementation, the piecewise quadratic polynomial approximation of Gerasoulis (1982) is adopted. This method, however, requires some modifications which are described below.

In an effort to obtain exact expressions for the integrals, Gerasoulis (1982), as well as others, approximates by polynomials not only the unknown singularity densities [here, $\tilde{\phi}(\chi, s)$ and $\tilde{D}_t(\chi, s)$] but also their product with the kernels (for example, $\tilde{\phi}(\chi, s)F_1(x-\chi, s)$). In other words, on a quadratic element with two end nodes located at χ_{2k-2} and χ_{2k}, such a product can be expressed as

$$\tilde{\phi}(\chi, s)F_1(x-\chi, s) \cong \sum_{i=2k-2}^{2k} \mathscr{L}_i(\chi)\tilde{\phi}(\chi_i, s)F_1(x-\chi_i, s), \tag{B1}$$

where $\mathscr{L}_i(\chi)$ are shape functions based on the Lagrangian polynomials

$$\mathscr{L}_i(\chi) = \prod_{\substack{j=2k-2 \\ j\neq i}}^{2k} \frac{\chi-\chi_j}{\chi_i-\chi_j}. \tag{B2}$$

Substituting the discretized form (B1) into the corresponding integral in (48), we obtain

$$\int_{\chi_{2k-2}}^{\chi_{2k}} \frac{\tilde{\phi}(\chi, s)F_1(x-\chi, s)}{\sqrt{L^2-\chi^2}}\,d\chi \cong \sum_{i=2k-2}^{2k} \tilde{\phi}(\chi_i, s)F_1(x-\chi_i, s)\int_{\chi_{2k-2}}^{\chi_{2k}} \frac{\mathscr{L}_i(\chi)}{\sqrt{L^2-\chi^2}}\,d\chi. \tag{B3}$$

The integral on the right-hand side of (B3) is independent of the kernel function F_1 and has been found analytically by Gerasoulis (1982).

This procedure, although very efficient and accurate in dealing with elastic crack problems, leads to a solution breakdown in the present application. The difficulty appears to be rooted in the inadequate approximation of the kernel functions F_i, $i = 1$–4 by (B1). The kernel functions are generally non-monotonic. The relative steepness of the peak in an element is controlled by two scaling factors: a fixed scale of the element size (for a fixed number of elements used in solution), and a variable one for the Bessel functions, measured as $\sqrt{c/s}$. For a typical problem, the value of s needs to be varied between 10^{-3} and 10^{5}. As s becomes large, a steep peak profile may be located on an element. Sampling the function at only three nodal points of the element can completely miss its characteristics. In the actual numerical implementation, the solution breaks down as soon as s approaches $10^{2}c/L^{2}$ for a limited number of elements. Reduction of the element size is not an effective measure as it cannot catch up with the rate of increase of s. A modification of the Gerasoulis procedure is therefore necessary.

At the cost of performing a numerical integration, eqn (B3) is cast in a different form

$$\int_{\chi_{2k-2}}^{\chi_{2k}} \frac{\tilde{\phi}(\chi,s)F_i(x-\chi,s)}{\sqrt{L^2-\chi^2}}\,d\chi \cong \sum_{i=2k-2}^{2k} \tilde{\phi}(\chi_i,s)\int_{\chi_{2k-2}}^{\chi_{2k}} \frac{\mathscr{L}_i(\chi)F_i(x-\chi_i,s)}{\sqrt{L^2-\chi^2}}\,d\chi. \tag{B4}$$

Using a numerical quadrature, a large number of sampling points can be distributed to capture the variation of the function. The procedure adopted herein is the DCADRE subroutine of the IMSL (1985) library, which is based on an adaptive Romberg extrapolation procedure that automatically executes to a user-specified accuracy. With this improvement in the program, no difficulty was experienced in carrying out the solution into the small time (large s) range.

To find the numerical solution, the integral equations with a pre-assigned s value were discretized into N quadratic elements ($2N+1$ nodes). The system involves $4N+2$ unknowns. To generate the linear system of equations, the stress equation in (48) is collocated for the known normal stress boundary condition at the $2N$ nodes located at the quarter and three-quarter length of each element. The pressure equation is collocated at $2N+1$ nodes distributed at equal distances over the fracture length, which generally do not coincide with the stress nodes. These $4N+1$ equations, combined with the auxiliary closure condition (43), produce just enough equations for the solution of the linear system. The discrete solutions of $\tilde{\phi}$ and $\tilde{D}_i$ can then be integrated to produce other quantities of interest, such as the fracture displacement, fracture volume, fluid leak-off volume, etc.

Once the integral equations (48) and (43) have been solved in terms of the Laplace transform of ϕ and D_i using the procedure described above, a numerical inversion technique is applied to find the solution in time. The algorithm adopted here is the method of Stehfest (1970), which requires evaluation of the transform solution for real values of the transform parameter only: letting $\tilde{f}(s)$ be the transform of $f(t)$ which can be determined for any discrete value of s, then the approximate solution in the time domain is computed according to

$$f(t) \approx \frac{\ln 2}{t}\sum_{n=1}^{N} C_n \tilde{f}\left(n\frac{\ln 2}{t}\right), \tag{B5}$$

with the coefficient C_n given by

$$C_n = (-1)^{n+N/2}\sum_{k=(n+1)/2}^{\min(n,N/2)} \frac{k^{N/2}(2k)!}{(N/2-k)!\,k!\,(k-1)!\,(n-k)!\,(2k-n)!}. \tag{B6}$$